Numerical and experimental investigation of propeller noise with trailing-edge serrations

Bin Zang* and Liam Hanson†
Faculty of Engineering, University of Bristol, BS8 1TR, United Kingdom

Aimee Stoltz‡ , Wei Hua Ho§
University of Witwatersrand, Braamfontein 2000, Johannesburg, South Africa

Xiao Liu¶ and Mahdi Azarpeyvand‖
Faculty of Engineering, University of Bristol, BS8 1TR, United Kingdom

The present study examines the effect of trailing-edge serrations on propeller noise at both hover and forward flight conditions. Three different serrations were designed with wavelength-to-amplitude ratios from 0.6 to 1.2, based on the several recent literature. Both experimental measurement and numerical simulations were carried out to first quantify the far-field noise spectra and subsequently, to provide flow field analyses, which can shed some lights on the physical mechanisms leading to the noise reduction at different operating conditions. The results show that the present unsteady RANS simulation predicts the far-field acoustics of both the baseline and serrated propellers, which agree relatively well with the experimental measurements at hover conditions. However, due to limited simulation time, the blade pass frequencies and its harmonics are not well captured. Moreover, the use of trailing-edge serrations on propellers lead to clear reduction of the far-field noise levels, and the effectiveness of the noise reduction is dependent on the key parameters defining the serrations as well as the propeller operating condition. With the serrations, the turbulent kinetic energy over the entire blade reduces, particularly close to the trailing-edge regions and the iso-surface contours reveal that the turbulent structures become less coherent in the blade spanwise direction. Subsequently, these turbulent structures are observed to decay more rapidly than the baseline configuration in the near-wake region. These modifications to the turbulent structures on the blade as well as in the near-wake possibly contributes the reduction of far-field noise by applying trailing-edge serrations to the propellers.

I. Nomenclature

CFD	=	Computational Fluid Dynamics
D	=	propeller diameter [mm]
FW-H	=	Ffowc-William-Hawking
OASPL	=	overall sound pressure level
P	=	propeller pitch [mm]
RANS	=	Reynolds-Averaged Navier-Stokes
Re_c	=	Reynolds number based on the chord length at 75% of the span
SPL	=	sound pressure level [dB]
TKE	=	turbulent kinetic energy
U_∞	=	free-stream velocity [m/s]
U_t	=	total velocity [m/s]

*Lecturer, Department of Aerospace Engineering, AIAA Member
†PhD Candidate, Department of Aerospace Engineering
‡Undergraduate student, School of Mechanical, Industrial and Aeronautical Engineering
§Associate Professor, School of Mechanical, Industrial and Aeronautical Engineering
¶Wind Tunnel Technical Specialist, Department of Aerospace Engineering
‖Professor of Aerodynamics and Aeroacoustics, Department of Aerospace Engineering

c	=	propeller chord [mm]
c_{mac}	=	mean aerodynamic chord of the propeller span [mm]
$c_{75\%}$	=	propeller chord at 75% of the propeller span [mm]
f	=	frequency [Hz]
h	=	serration amplitude [mm]
p'	=	pressure fluctuations
$\bar{u'}$, $\bar{v'}$, $\bar{w'}$	=	velocity fluctuations component along the x, y and z-directions [m/s]
x, y, z	=	streamwise, cross-stream and spanwise directions of the computational domain
δ_t	=	timesteps size [s]
λ	=	serration wavelength [mm]

II. Introduction

The aviation industry has seen rapid development in urban air mobility (UAM) and unmanned aerial vehicle (UAV) technologies in recent years. These technologies offer promising potential in improving mobility and accessibility in the modern society. Unlike conventional aircraft propulsion system, these aerial vehicles are primarily driven by propellers with either hybrid or fully electric powertrain, which are often operated at a different flow regimes (*i.e.*, Reynolds numbers). More importantly, nature of their mission means that they are regularly operated close to the populous community, where reducing the vehicle and the associated propulsion noise becomes essential in achieving public and regulatory acceptance [1].

For a rotating propeller, several aerodynamic noise sources have been identified from the previous studies [2], such as tones from the periodic rotation of the propeller blades as well as the broadband noise from turbulence. The latter consists of mainly the trailing-edge noise, which is generated via the scattering of a turbulent boundary layer by the sharp trailing edge [3]. Chen *et al.* [4] developed a semi-empirical noise prediction framework for small-scale rotors and concluded that trailing-edge noise is the primary component of the broadband noise for the rotors [4]. At a much larger scale, Oerlemans *et al.* [5] also found that the trailing-edge noise is the dominant broadband noise source for a utility-scale wind turbines. Therefore, it is reasonable to argue that reducing trailing-edge noise can effectively attenuate the broadband noise generated from a rotating propeller and hence, reducing the overall noise emission of the propulsion system for the UAM/UAV vehicles.

Inspired by nature, such as the Owl's wing, significant amount of research have been focused on the design and use of serrated trailing-edges to reduce the scattered noise. Through analytical, experimental and numerical investigations of a range of serrations [6–8], two mechanisms were proposed to contribute to the reduction of trailing-edge noise by serrations: firstly, it was shown by Howe [9, 10] and later confirmed by Lyu *et al.* [11] that the serrations reduce the noise scattering by destructive interference and secondly, several studies [6, 12] have demonstrated that the production of a counter-rotating vortex pair at the sides of the serration, which contributed to the mitigation of the trailing-edge noise, likely due to enhanced mixing.

Trailing-edge serrations has also been applied to the propeller blades in an attempt to reduce the broadband noise. Ning *et al.* [13] investigated the aerodynamic and aeroacoustic characteristics of UAV rotors. They applied sawtooth serrations with four different wavelength-to-amplitude ratios to the full span of the UAV propellers and experimentally quantified their aerodynamic and aeroacoustic performances. The results showed that compared to the straight trailing edge (the baseline), the trailing-edge serrated blades produce approximately 0.9 to 1.6dB of reduction in overall sound pressure levels, while maintaining a similar thrust. Later, Yang *et al.* [14] performed noise and flow measurements for the propellers with trailing-edge serrations applied to both half and full span at chord-based low Reynolds number in the order of 10^5 and observed that similar levels of noise reduction were achieved between the two. They attributed the similar performance to the fact that the tangential velocity was much higher for the outer region of the blades (*i.e.*, close to the blade tip) than that of the regions closer to the root, and hence were responsible for the noise generation, and in the case of serrated trailing-edge, the more effective noise reduction. Moreover, they argued from the 2D flow measurements that the reduced wake turbulence may also play a role in the reduction of blade-vortex interaction noise. Intravartolo *et al.* [15] examined the effects of 'cut-in' amplitudes on the overall noise reduction of trailing-edge serrated propellers and found that an optimal balance between the aerodynamic performance and noise mitigation was approximately 28% of the mean aerodynamic chord.

Compared to a static wing, the noise generation mechanisms of a propeller is significantly more complex and hence, it is important to further improve our understanding of the physical mechanisms leading to the noise mitigation observed with trailing-edge serrated propellers, so that optimal serrations, suitable for different flow regimes, can potentially be

designed and applied to engineering applications. The present study intends to combine both numerical simulations and experimental measurements to shed more light on the performance and mechanisms of noise reduction for different trailing-edge serrations at hover and forward flight conditions. The remainder of this paper is organised as follows: descriptions of the numerical and experimental set-up, including a brief introduction of the methodologies is followed by the discussion of results at both hover and forward flight, before outlining the conclusion and prospective work.

III. Set-up and Methodologies

A. Propeller geometry with trailing-edge serrations

In the present study, a two-bladed $12'' \ (P) \times 18'' \ (D)$ composite-fibre propeller was used. The propeller diameter, D, is 30 mm and has a relative constant chord up to 60% of the span. The mean aerodynamic chord, c_{mac} is thus comparable to that of the chord at 75% of the propeller span, $c_{75\%}$, and $c_{75\%}$ =14 mm. In order to design effective trailing-edge serrations for reducing the noise, some key parameters associated with the serration should be considered, namely the amplitude, $2h$, and the wavelength, λ. Figure 1 shows the three different trailing-edge serrations chosen for the study, with the respective definitions of amplitude and wavelength. According to Intravartolo *et al.* [15], the optimal ratio between the amplitude ($2h$) of the serrations and the mean aerodynamic chord was approximately 28%. Moreover, based on Howe's [9, 10] analytical model, it was also suggested that the wavelength-to-amplitude ratio (λ/h) should also be kept below 4. Therefore, three different wavelengths from 1.2 mm to 2.4 mm were selected with a constant amplitude of $2h$ = 4 mm, so that the resulting serrations cover the range of wavelength-to-amplitude ratio from λ/h = 0.6 to λ/h = 1.2. Ning *et al.* [13] used similar serration geometries in their propeller study and showed that such serrations are effective in reducing the overall noise levels of the propellers, operating at similar conditions. Table 1 summarises the geometric parameters of the three serrations used.

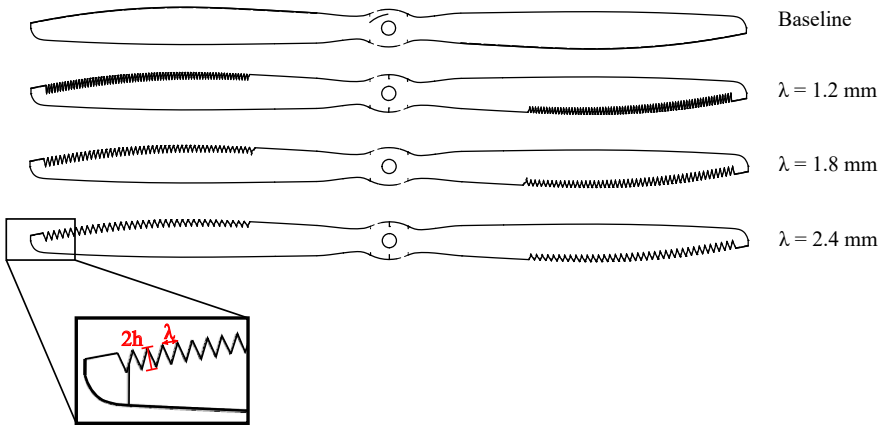

Fig. 1 Geometry of the baseline and trailing-edge serrated propeller blades. Three different serrations profiles of λ/h =0.6, 0.9 and 1.2 were chosen.

Table 1 Description of the serration geometry for each of the 3 modified cases.

Name	Amplitude, $2h$ (mm)	Wavelength, λ (mm)	λ/h
Serration 1	4	1.2	0.6
Serration 2	4	1.8	0.9
Serration 3	4	2.4	1.2

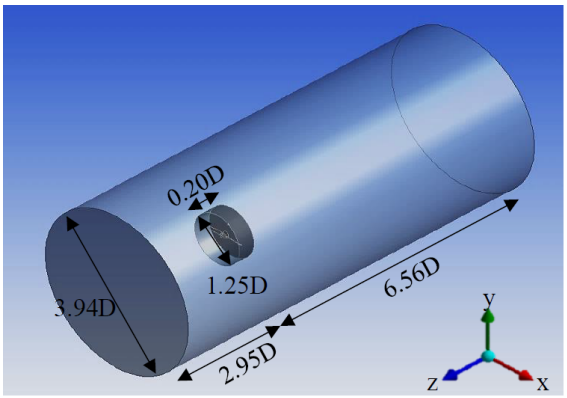

Fig. 2 Static and rotating domains of the numerical set-up.

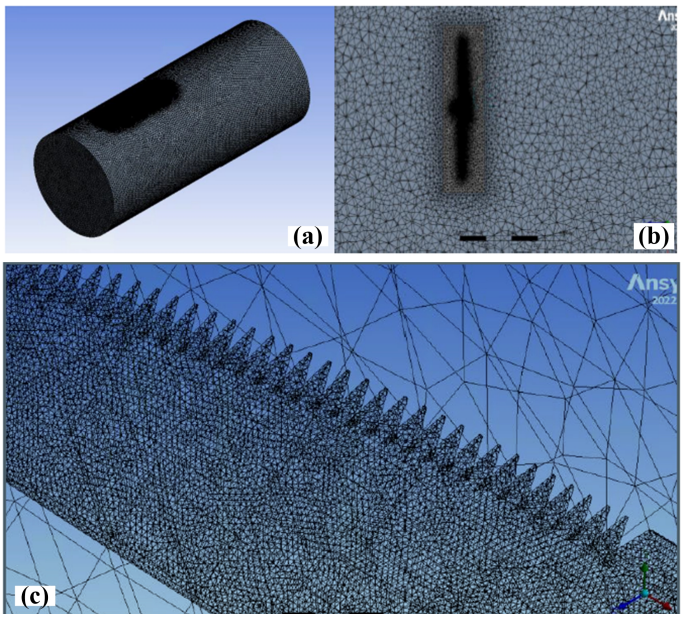

Fig. 3 Mesh topology of the numerical set-up for (a) Mesh of model (b) Sectioned view of rotary domain mesh containing the propeller blade (c) Sectioned view of the model geometry mesh (d) Baseline propeller blade surface mesh (e) Serrated propeller blade surface mesh.

B. Numerical set-up

Unsteady RANS (Reynolds-Averaged Navier-Stokes) simulations were undertaken utilising ANSYS Fluent 2022 to determine the flow and acoustic characteristics of the isolated two-bladed propeller at a fixed angular velocity of 4000 RPM at both hover and forward flight conditions, which the free-stream velocities were maintained at U_∞ =0 m/s and U_∞ =25 m/s, respectively. Sliding mesh method was adopted to simulate the rotation of the propeller. The overall domain consisted of two cylindrical sub-domains one inside the other, as shown in Fig. 2. The inner domain contains the propeller and where mesh motion, of 4000 RPM, was set.

To accurately capture the velocity field and the pressure fluctuations from the propeller (hence the propagated acoustic pressure), mesh refinement was carried out surrounding the propeller model as well as within the domain of rotation. Figure 3 shows the overall mesh typology and the zoomed-in views of the rotating domain and the propeller model, as seen in Fig. 2. Moreover, mesh convergence test was carried out with four different mesh resolutions from 2.2million to 6.4million. The acoustic results from the simulation of the baseline configuration (*i.e.*, no serration) were compared with that of experimental measurement at U_∞ =0 m/s. The differences of sound pressure level from 800 Hz to 8 kHz were evaluated and presented in Fig. 4, in terms of error percentage. Figure 4 illustrates that the present simulation

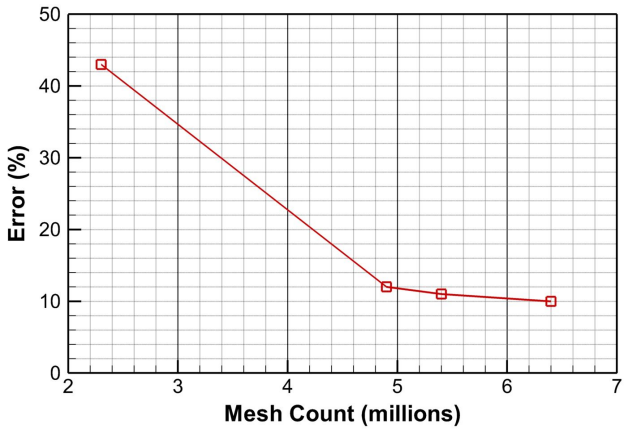

Fig. 4 Percentage of error of the far-field acoustics compared between the numerical simulations with different mesh resolution and the experiments for the baseline configuration at U_∞ =0 m/s.

achieves relatively constant percentage error with mesh sizes above 4.9 million cells, and based on the mesh convergence analysis, a mesh size of approximately 6.4million cells was determined suitable for all numerical simulations presented hereafter. Far-field noise was then computed with Ffowc-William-Hawking (FW-H) implementation, treating the solid propeller blades as the noise source. Acoustic receiver locations were placed at 15° intervals between 50° and 130°. A sphere of influence with denser mesh was used around the receiver locations.

A zero-gauge pressure or velocity inlet boundary conditions (BCs) was prescribed for the upstream of the propeller and zero-gauge pressure outlets were used for all other BCs. The propeller surface was standard no-slip wall condition. An interface boundary was used to for interface between the two sub-domains to allow for the flow between them. A total of 3000 time steps were run which is an equivalent of 0.6 RPM. This is due to computational resources. Table 2 below summarises the numerical set-up of the URANS simulations.

C. Experimental set-up

The experimental tests were performed in the aeroacoustic wind tunnel facility at the University of Bristol. The facility consists of an closed-circuit, open jet anechoic wind tunnel. The anechoic chamber has acoustically treated interiors, making it fully anechoic down to 160 Hz. The nozzle has a width of 500 mm and a height of 775 mm. The design permits steady operation from 5 m/s to 45 m/s with a normal turbulence intensity level below 0.2%. A complete description of the aeroacoustic wind tunnel facility can be seen in the work by Mayer *et al.* [16].

In the present investigation, the aeroacoustic performance of the different trailing-edge serrations was characterised by collecting far-field noise data. A 23-element azimuthal microphone array located 1.75 m from the propeller hub was used to collect far-field acoustic data, as shown in Fig. 5. The microphone array was fitted with ¼ inch diameter G.R.A.S 40PL free-field microphones at polar angles between 40° − 150°. Each of the GRAS 40PL microphones has an upper limit of 142 dB and cover a frequency range between 10 Hz to 20 kHz. The propeller was oriented in the centre of the nozzle located in a plane 600 mm downstream from the nozzle exit, as shown in Fig. 5. The collected far-field acoustic pressure information was then used to obtain the sound pressure level of the noise as: $SPL = 10log_{10}(p'^2/{p_0}^2)$, where p'^2 are the magnitude squared pressure fluctuations calculated via the Welch's function and p_0 =20 µm denotes the reference pressure. Subsequently, the overall sound pressure level is determined by integrating the sound pressure level over a frequency range of 160 Hz $\leq f \leq$ 10 kHz.

The propeller was driven by a 40 A T-Motor Antigravity MN4006 brushless DC motor. The motor throttle was controlled through the use of an electronic speed controller (ESC) which changed the rotational rate of the propeller. A PCB electronics LaserTach LT2-ICP tachometer was used to provide a one-per-revolution feedback signal to the RPM control system implemented in National Instruments LabView. Aerodynamic loads were measured by a 6-component ATI mini40 multi axis load cell fitted directly behind the motor; giving an isolated load path. The test rig used in this study has been previously utilised in previous experiments which can offer further information on the test rig and setup [17–22].

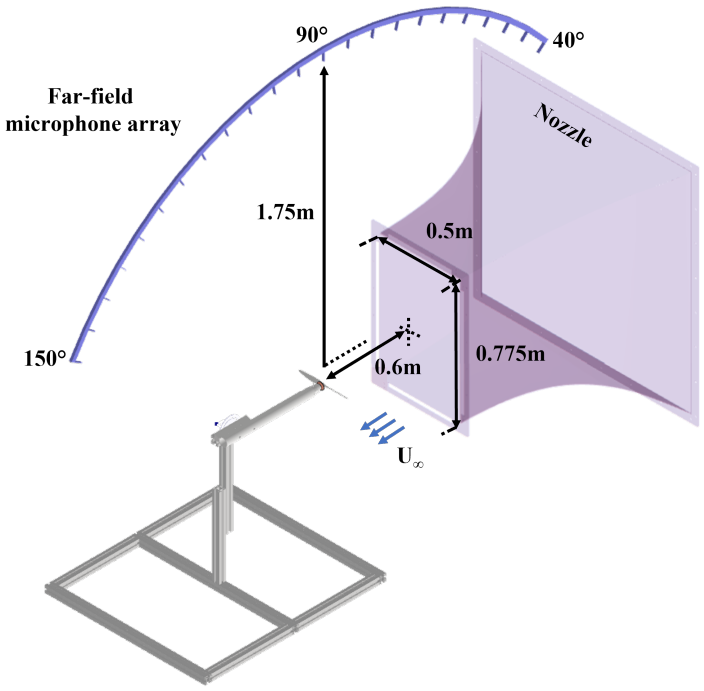

Fig. 5 Experimental set-up in the aeroacoustic wind tunnel facility.

Table 2 Numerical boundary conditions

Turbulence Model	$k-\omega$
Rotation Model	Sliding mesh method
Cell zone condition	Rotating domain - mesh motion
Solution method	SIMPLE
Timestep size, δt (s)	3×10^{-6}
Number of timesteps	3000
Simulation run time (hours)	50

IV. Results and discussion

A. far-field noise measurement

To first examine and understand the effectiveness of the trailing-edge serrations on reducing the propeller noise, Figs. 6 and 7 show the far-field noise spectra of both the baseline and three different trailing-edge serrated propellers at hover (i.e., U_∞ =0 m/s) and forward flight (i.e., U_∞ =25 m/s). Note that for both operating conditions, the rotational speed of propeller was kept constant at 4000 RPM. The latter corresponds to an advance ratio, $J = U_\infty/nD$ = 1.25 and Reynolds number of $Re_c = U_\infty c_{75\%}/\nu \approx$ 23,000.

At hover condition, as seen in Fig. 6, the far-field noise spectra shows the typical characteristics with a combination of tonal peaks at fundamental and harmonics of the blade pass frequency as well as a broadband hump at mid-frequencies from 500 Hz $\leq f \leq$ 2000 Hz approximately, before a relatively linear decay at high frequencies. The trailing-edge serrated propellers appear to exhibit similar characteristics to those of the baseline, however, all three serrations show signs of noise reduction, beginning from the first harmonic and persisting across the entire frequency range investigated. More importantly, serrations with moderate wavelength-to-amplitude ratio, λ/h =0.9, outperforms both the serrations with λ/h =0.6 (*i.e.*, narrower serration shape with sharper inclination angle) and with λ/h =0.9 (*i.e.*, wider serration shape with blunter inclination angle). This is in general agreement with the analytical analyses from Lyu *et al.* [11]

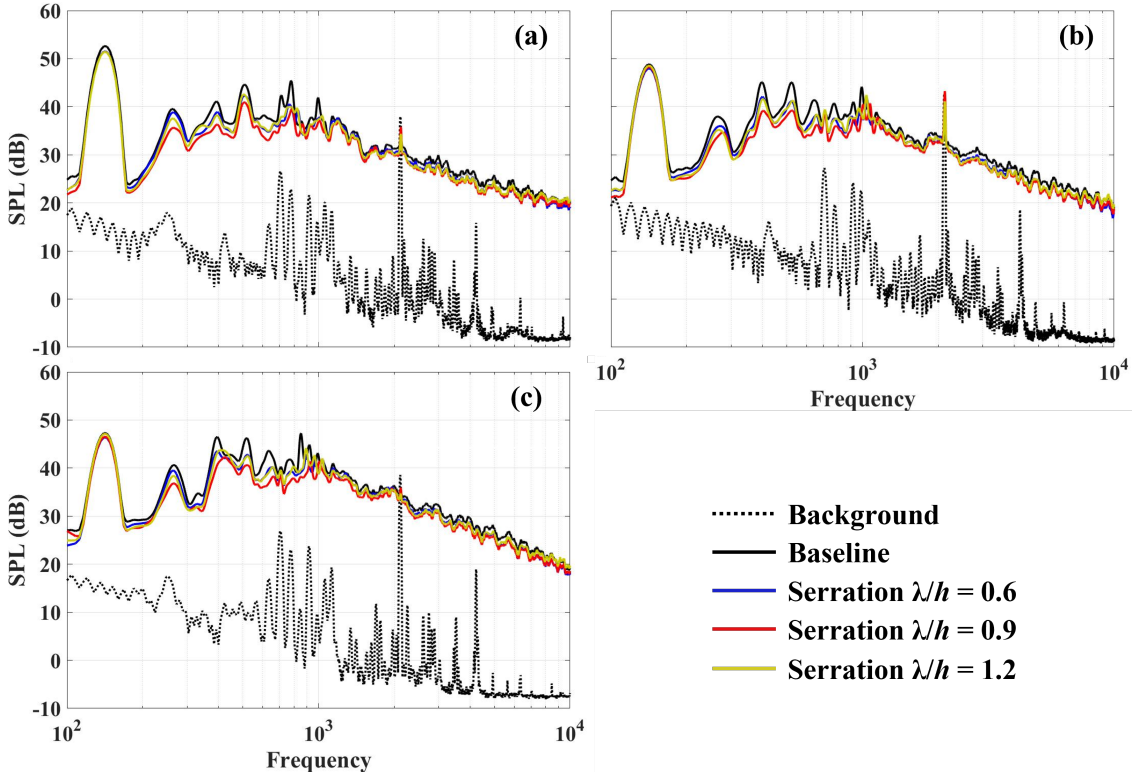

Fig. 6 Far-field noise spectra of both the baseline and three different trailing-edge serrated propellers at hover, U_∞ =0 m/s, for polar angles of (a) 50°, (b) 90° and (c) 130°, respectively.

that the sharper serrations enhance the noise mitigation ability, and yet there existed a limit (meaning 'sharp enough'). Interestingly, even though the trailing-edge serrations are designed to reduce the broadband noise scattered from the trailing-edge, it is also shown to attenuate the tonal peaks at multiples of the blade pass frequencies.

When the free-stream velocity increases to U_∞ =25 m/s, the far-field noise can be seen to be mostly dominated by the flow noise from the nozzle itself. Nevertheless, a closer examination of the noise spectra at high frequencies, $f \geq$3000 Hz, where the propeller SPLs are sufficiently higher than that of the flow, a glimpse of noise reduction from the trailing-edge serrations can be observed as compared to the baseline. This is consistent with the studies in the literature. Figure 8 shows the overall sound pressure levels over the full polar angles of $40° - 150°$. Consistent with the individual frequency-dependent spectra at distinct angles, the OASPL results reaffirms that the trailing-edge serrated propellers are capable of reducing the overall sound pressure levels by about 2 to 3 dB at hover flight condition. However, at forward flight condition and a propeller rotational speed of 4000 RPM, the effects of serrations are masked by the presence of dominant nozzle flow noise.

Figures 9 and 10 show the comparison of the far-field noise computed from the unsteady RANS simulation with that from the experimental measurements at both hover and forward flight conditions, for the baseline and λ/h =0.9 trailing-edge serrated propellers. It is useful to recall that since the simulations data were collected only for 3000 timesteps due to computational resource limits, the noise spectra at lower frequencies cannot be resolved and compared quantitatively. However, at frequencies higher than $f \geq$600 Hz, the comparison shows good agreement between the numerical simulations and the experiments, both in terms of the trend and of the absolute magnitude. Furthermore, it can be seen from the numerical results that the trailing-edge serrations lead to reduction in the far-field noise over the entire range of frequencies investigated, consistent with the experiments. On the other hand, the noise predicted from the forward flight condition becomes less reliable as the fluctuation of the SPL becomes noticeable and deviates from that of the experiments.

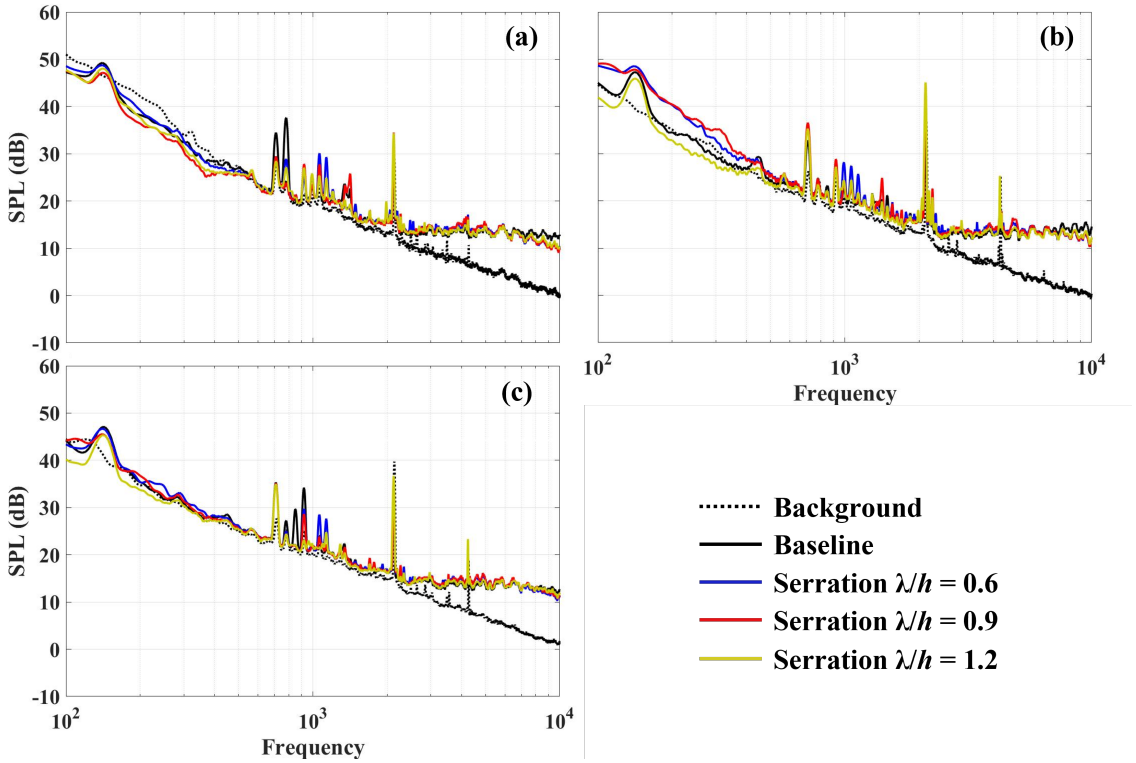

Fig. 7 Far-field noise spectra of both the baseline and three different trailing-edge serrated propellers at forward flight, U_∞ =25 m/s, for polar angles of (a) 50°, (b) 90° and (c) 130°, respectively.

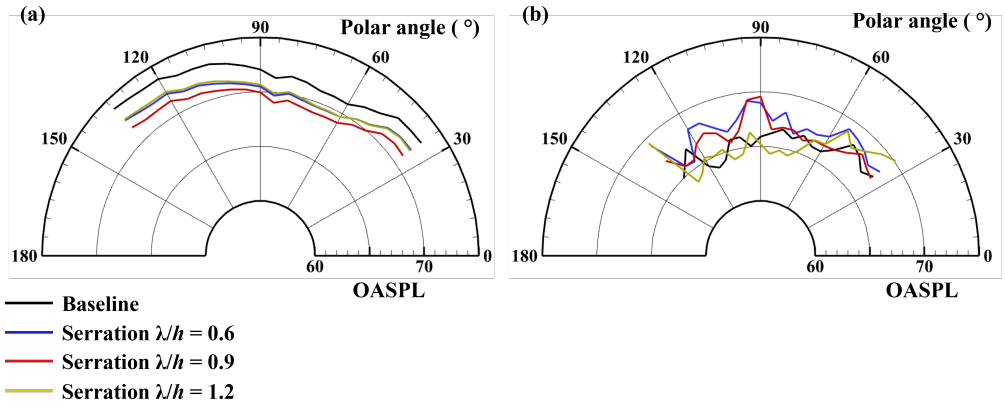

Fig. 8 Overall sound pressure levels of the baseline and three trailing-edge serrated propellers for (a) hover flight, U_∞ =0 m/s and (b) forward flight, U_∞ =25 m/s.

B. Near-field flow characteristics

To reveal the flow field characteristics that can directly contribute to the physical mechanisms of noise reduction by the trailing-edge serrations, Figs. 11 and 12 show the iso-surfaces of turbulent kinetic energy close to the propeller blade surface and the total velocity magnitude in the propeller wake for the baseline and λ/h =0.9 trailing-edge serrated propellers, respectively. The turbulent kinetic energy (TKE) is defined as $\frac{1}{2}(\bar{u'}^2 + \bar{v'}^2 + \bar{w'}^2)$, where $\bar{u'}$, $\bar{v'}$ and $\bar{w'}$ are the mean velocity fluctuation component along the x, y and z-directions. From Fig. 11, it can be seen that compared to the baseline case, the trailing-edge serrated propeller produces a lower TKE level with less coherent flow structures along the spanwise direction close to the trailing-edge regions. According to the Amiet's theory on trailing-edge noise [23],

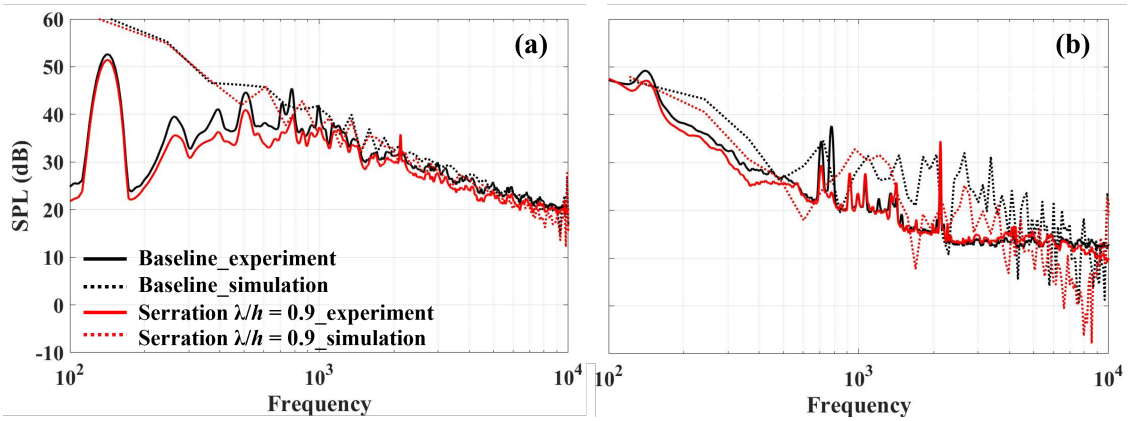

Fig. 9 Comparison of the far-field noise computed from the unsteady RANS simulation with the experiment at polar angle of 50° for (a) hover flight, U_∞ =0 m/s and (b) forward flight, U_∞ =25 m/s.

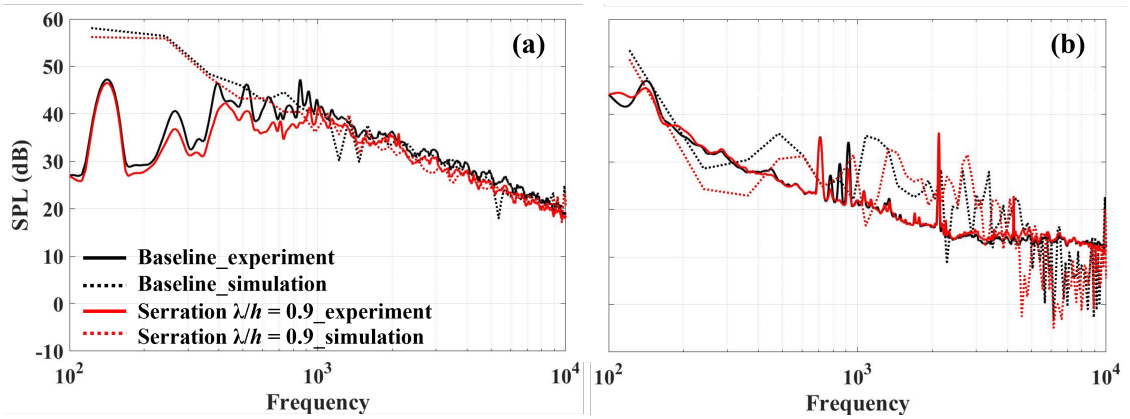

Fig. 10 Comparison of the far-field noise computed from the unsteady RANS simulation with the experiment at polar angle of 130° for (a) hover flight, U_∞ =0 m/s and (b) forward flight, U_∞ =25 m/s.

the lower turbulent fluctuations coupled with diminished spanwise coherence would directly yield reduction of the trailing-edge noise for the serrated blades, which corroborates with the far-field acoustic results. A closer examination of the TKE distribution reveals that the serrations are likely to influence overall TKE distribution over the entire blades, indicated by smaller regions of concentrated iso-surfaces of the trailing-edge serrated propellers as compared with the baseline configuration. The flow field results in the wake of the propellers, as shown in Fig. 12 agrees well with those observed close to the blade surface, which the wake flow dissipates more quickly for the trailing-edge serrated case. Moreover, the velocity contours are much less uniform for the serrated case, suggesting either a faster break-down of the wake structures or considerably less uniformity in the spanwise direction. These observations from the turbulent kinetic energy distribution over the blades and the decay of the wake velocity profiles provides some possible explanations to the noise reduction of the trailing-edge serrated propellers.

V. Concluding remark and prospective work

The paper presents a preliminary study to reduce propeller noise at both hover and forward flight conditions by applying trailing-edge serrations to the propeller. The results show that the use of trailing-edge serration on propellers can lead to clear reduction of the far-field noise level at hover flight conditions, and likely at forward flight. The effectiveness of the noise reduction is dependent on the key parameters defining the serrations, namely the wavelength-to-amplitude ratio of the serration. For the present study, a trailing-edge serration with λ/h=0.9 produces the best noise reduction performance across the full range of frequencies investigated. Therefore, trailing-edge serration is a potentially viable noise reduction technique which warrants further investigation. Unsteady RANS simulation has also been successfully

carried out with acoustic prediction using FW-H formulation. The simulation results show promising ability when the resulting noise spectra are compared with the experiments. Moreover, the flow field analysis on the blades and in the near-wake region of the propeller blades illustrate that serrations can reduce the turbulent kinetic energy level over the trailing-edge of the blade as well as the spanwise coherence of the turbulent structures, and subsequently lead to faster, less uniform velocity decay in the near-wake region, which partly explains the reduction of far-field noise with trailing-edge serrated propellers. To further correlate the flow development with the noise generation process of the serrated blades as well as to elucidate the detailed mechanisms leading to the noise reduction, higher fidelity numerical simulations will be conducted in the prospective work.

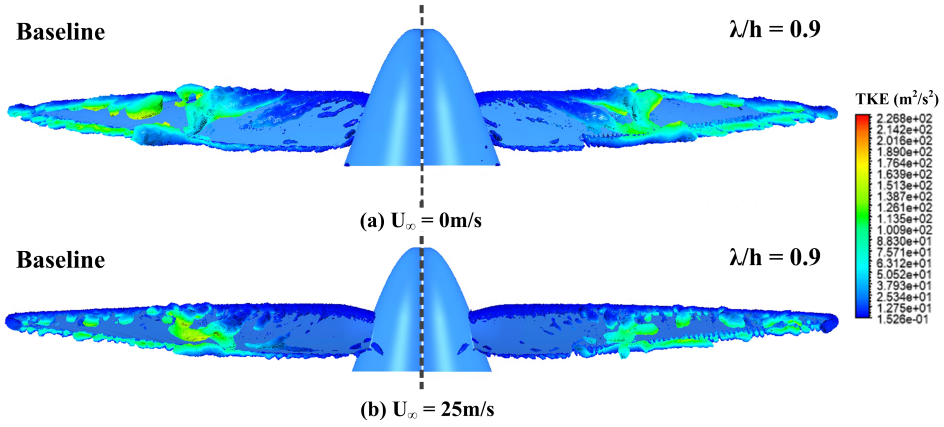

Fig. 11 Comparison of the turbulence kinetic energy distribution near the blade surface between the baseline and $\lambda/h = 0.45$ serrations for the (a) hover flight at U_∞ =0 m/s (b) forward flight at U_∞ =25 m/s.

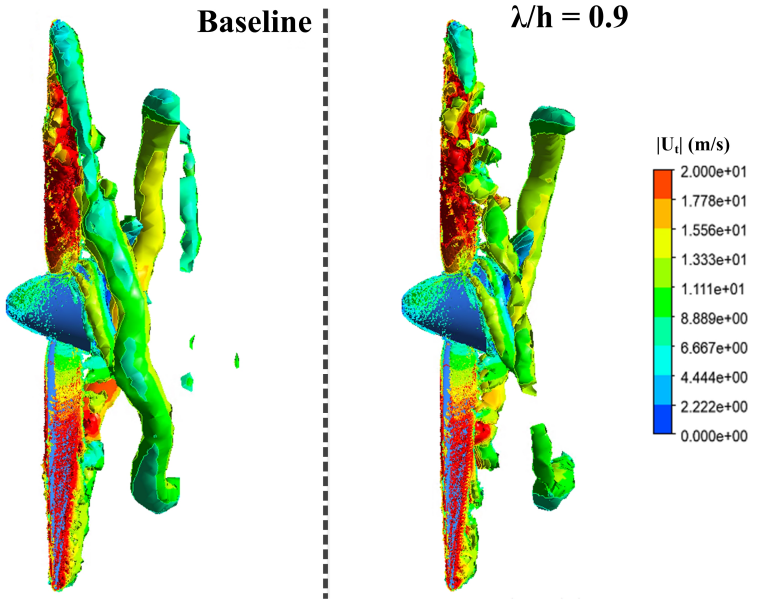

Fig. 12 Comparison of the development of the wake profile (in velocity iso-surface) between the baseline and $\lambda/h = 0.45$ serrations for forward flight at U_∞ =25 m/s.

References

[1] Rizzi, S. A., Huff, D. L., Boyd, D. D., Bent, P., Henderson, B. S., Pascioni, K. A., Sargent, C., Josephson, D. L., Marsan, M., He, H. B., et al., "Urban Air Mobility Noise: Current Practice, Gaps, and Recommendations," Tech. Rep. TP-20205007433, Hampton, Virginia, 2020.

[2] Jack, E., and Kurtz, D. W., "A Review of Aerodynamic Noise From Propellers, Rotors, and Lift Fans," Tech. Rep. NASA-CR-107568, Pasedena, California, 1970.

[3] Brooks, T. F., Pope, D. S., and Marcolini, M. A., "Airfoil Self-noise and Prediction," Tech. Rep. NASA-RP-1218, Hampton, Virginia, 1989.

[4] Chen, L., Batty, T., Giacobello, M., and Widjaja, R., "Prediction of Small-scale Rotor Noise Using a Low-fidelity Model-based Framework," *Proceedings of ACOUSTICS*, Vol. 10, 2019.

[5] Oerlemans, S., Fisher, M., Maeder, T., and Kögler, K., "Reduction of Wind Turbine Noise Using Optimized Airfoils and Trailing-Edge Serrations," *AIAA Journal*, Vol. 47, No. 6, 2009, pp. 1470–1481.

[6] Avallone, F., Pröbsting, S., and Ragni, D., "Three-dimensional Flow Field over a Trailing-edge Serration and Implications on Broadband Noise," *Physics of Fluids*, Vol. 28, No. 11, 2016, p. 117101.

[7] Arce León, C., Merino-Martínez, R., Ragni, D., Avallone, F., Scarano, F., Pröbsting, S., Snellen, M., Simons, D. G., and Madsen, J., "Effect of Trailing Edge Serration-Flow Misalignment on Airfoil Noise Emissions," *Journal of Sound Vibration*, Vol. 405, 2017, pp. 19–33.

[8] Avallone, F., Van Der Velden, W., Ragni, D., and Casalino, D., "Noise Reduction Mechanisms of Sawtooth and Combed-sawtooth Trailing-edge Serrations," *Journal of Fluid Mechanics*, Vol. 848, 2018, pp. 560–591.

[9] Howe, M. S., "Noise Produced by a Sawtooth Trailing Edge," *The Journal of the Acoustical society of America*, Vol. 90, No. 1, 1991, pp. 482–487.

[10] Howe, M. S., "Aerodynamic Noise of a Serrated Trailing Edge," *Journal of Fluids and Structures*, Vol. 5, No. 1, 1991, pp. 33–45.

[11] Lyu, B., Azarpeyvand, M., and Sinayoko, S., "Prediction of Noise from Serrated Trailing Edges," *Journal of Fluid Mechanics*, Vol. 793, 2016, pp. 556–588.

[12] Chong, T. P., and Vathylakis, A., "On the Aeroacoustic and Flow Structures Developed on a Flat Plate with a Serrated Sawtooth Trailing Edge," *Journal of Sound and Vibration*, Vol. 354, 2015, pp. 65–90.

[13] Ning, Z., Wlezien, R. W., and Hu, H., "An Experimental Study on Small UAV Propellers with Serrated Trailing Edges," *47th AIAA fluid dynamics conference*, Denver, Colorado, 2017, pp. 2017–3813.

[14] Yang, Y., Wang, Y., Liu, Y., Hu, H., and Li, Z., "Noise Reduction and Aerodynamics of Isolated Multi-copter Rotors with Serrated Trailing Edges during Forward Flight," *Journal of Sound and Vibration*, Vol. 489, 2020, p. 115688.

[15] Intravartolo, N., Sorrells, T., Ashkharian, N., and Kim, R., "Attenuation of Vortex Noise Generated by UAV Propellers at Low Reynolds Numbers," *55th AIAA Aerospace Sciences Meeting*, Grapevine, Texas, 2017, pp. 2017–2019.

[16] Mayer, Y. D., Jawahar, H. K., Szőke, M., Ali, S. A. S., and Azarpeyvand, M., "Design and performance of an aeroacoustic wind tunnel facility at the University of Bristol," *Applied Acoustics*, Vol. 155, 2019, pp. 358–370. https://doi.org/10.1016/j.apacoust.2019.06.005.

[17] Zhou, B. Y., Hanson, L. P., Pullin, S. F., Zang, B., Hauth, J., and Huan, X., "A Data-Driven Approach for Enhancement of Propeller Performance Prediction," *28th AIAA/CEAS Aeroacoustics 2022 Conference*, 2022, p. 3106.

[18] Hanson, L. P., Baskaran, K., Zang, B., and Azarpeyvand, M., "Aeroacoustic Interactions of a Trailing Edge Mounted Propeller and Flat Plate," *28th AIAA/CEAS Aeroacoustics 2022 Conference*, 2022, p. 2937.

[19] Hanson, L. P., Baskaran, K., Zang, B., and Azarpeyvand, M., "Acoustic Shielding and Scattering Effects of a Propeller Mounted Above a Flat Plate," *51st International Congress and Exposition on Noise Control Engineering*, 2022.

[20] Hanson, L. P., Baskaran, K., Pullin, S. F., Zhou, B. Y., Zang, B., and Azarpeyvand, M., "Aeroacoustic and Aerodynamic Characteristics of Propeller Tip Geometries," *28th AIAA/CEAS Aeroacoustics 2022 Conference*, 2022, p. 3075.

[21] Jamaluddin, N. S., Celik, A., Baskaran, K., Rezgui, D., and Azarpeyvand, M., "Aerodynamics and Aeroacoustics Characterisation of Isolated Rotor in Hover and Transition to Forward Flight," *AIAA AVIATION 2021 FORUM*, 2021, p. 2311.

[22] Jamaluddin, N. S., Celik, A., Baskaran, K., Rezgui, D., and Azarpeyvand, M., "Aeroacoustic Performance of Propellers in Turbulent Flow," *AIAA AVIATION 2021 FORUM*, 2021, p. 2188.

[23] Amiet, R. K., "Noise due to Turbulent Flow past a Trailing Edge," *Journal of Sound and Vibration*, Vol. 47, No. 3, 1976, pp. 387–393.